Dirac Node Lines in Pure Alkali Earth Metals

Ronghan Li,[1] Hui Ma,[1] Xiyue Cheng,[1] Shoulong Wang,[1] Dianzhong Li,[1] Zhengyu Zhang,[2] Yiyi Li,[1] and Xing-Qiu Chen[1,*]

[1]*Shenyang National Laboratory for Materials Science, Institute of Metal Research, Chinese Academy of Science, School of Materials Science and Engineering, University of Science and Technology of China, 110016 Shenyang, Liaoning, People's Republic of China*

[2]*International Center for Quantum Design of Functional Materials, Hefei National Laboratory for Physical Sciences at the Microscale and Synergetic Innovation Center of Quantum Information and Quantum Physics, University of Science and Technology of China, Hefei, Anhui 230026, People's Republic of China*

(Received 26 March 2016; published 22 August 2016)

Beryllium is a simple alkali earth metal, but has been the target of intensive studies for decades because of its unusual electron behavior at surfaces. The puzzling aspects include (i) severe deviations from the description of the nearly free-electron picture, (ii) an anomalously large electron-phonon coupling effect, and (iii) giant Friedel oscillations. The underlying origins for such anomalous surface electron behavior have been under active debate, but with no consensus. Here, by means of first-principles calculations, we discover that this pure metal system, surprisingly, harbors the Dirac node line (DNL) that in turn helps to rationalize many of the existing puzzles. The DNL is featured by a closed line consisting of linear band crossings, and its induced topological surface band agrees well with previous photoemission spectroscopy observations on the Be (0001) surface. We further reveal that each of the elemental alkali earth metals of Mg, Ca, and Sr also harbors the DNL and speculate that the fascinating topological property of the DNL might naturally exist in other elemental metals as well.

DOI: 10.1103/PhysRevLett.117.096401

Topological semimetals [1] represent new types of quantum matter, currently attracting widespread interest in condensed matter physics and materials science. Compared with normal metals, topological semimetals [1] are distinct in two essential aspects: the crossing points of the energy bands occur at Fermi level, and some of the crossing points consist of the monopoles in the lattice momentum space. Topological semimetals can be classified into three categories: topological Dirac (TD) [2], topological Weyl (TW) [3], and Dirac node line (DNL) semimetals [4–6]. In the former two cases of TD and TW, the monopoles form isolated points in the lattice momentum space and novel surface states (i.e., surface Dirac cones and Fermi-arc states) were observed or suggested, such as TD-type Na_3Bi [7–10] and Cd_3As_2 [11–13] and TW-type TaAs family [14–17] and TW-type-II WTe_2 [18].

In the third class of DNL, the crossings between energy bands form a fully closed line nearly at the Fermi level in the lattice momentum space, drastically different from the isolated Dirac (or Weyl) points in the TD and TW. According to the previous DNL modelings [4,5], the band crossings occur at zero energy with a constraint chiral symmetry, leading to the appearance of flat surface bands. However, in a real crystal the chiral symmetry of a band structure is not exact, thereby suggesting that the DNL does not generally occur at a constant energy and the DNL-induced topological surface bands are not flat either. Recently, this type of DNL state has been predicted in several cases of 3D carbon graphene allotropes [19], antiperovskite $Cu_3(Pd,Zn)N$ [20,21], Ca_3P_2 [22], LaN [23], photonic crystals [24], a hyperhoneycomb lattice [25], etc. But all these DNL predictions have yet to be experimentally verified. Here, we discover a new DNL state in beryllium, the first known example in pure metals. We find that the presence of the topologically protected (0001) surface states around the $\overline{\Gamma}$ point originates from this DNL state. Furthermore, realization of the existence of the DNL in principle offers new opportunities and insights in rationalizing the long-standing problem [26–34] of the pronounced surface states in Be.

The metal beryllium, which crystallizes in the hcp structure [35] [see Fig. 1(a)], is a simple sp-bonded metal. Be is unusual in three aspects. Firstly, at its bulk phase it is almost a semimetal, whereas its (0001) surface has well-defined, intense, and robust surface electronic states [26–28,33,34]. The surface states of simple metals were often interpreted within the framework of the nearly-free-electron (NFE) model [26]; however, beryllium behaves surprisingly far beyond this model. Secondly, the anomalous interplanar expansion [32], as large as $> 4\%$ of the topmost (0001) atomic layer, has been observed, different from most other pure metals which often show little relaxation or contraction when cracking into the surface. The underlying driving force for the lattice expansion has again been attributed to unusual electronic states at the surfaces [36,37]. Thirdly, the large electron-phonon

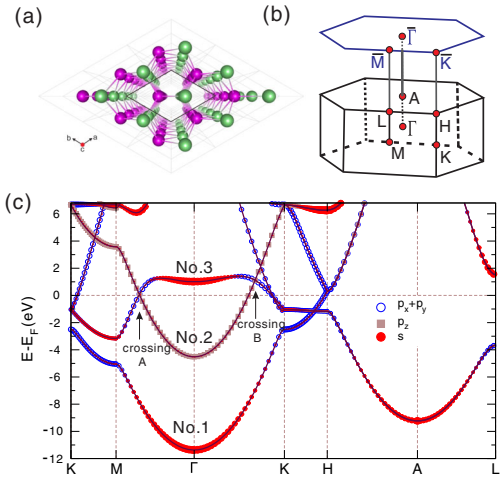

FIG. 1. Lattice structure and electronic band structure of hcp beryllium. (a) Crystal structure (here a $3 \times 3 \times 5$ supercell) (no. 194 $P63/mmc$ space group) with Be atom at the $2c$ site (1/3, 2/3, 1/4) in a perspective projection along the c axis. The layers consist of green and pink atoms alternatively stack along the c axis. (b) Brillouin zone (BZ) of the bulk phase and projected surface BZ of the (0001) surface. (c) Calculated electronic band structure along the high-symmetry points for the hcp Be bulk phase.

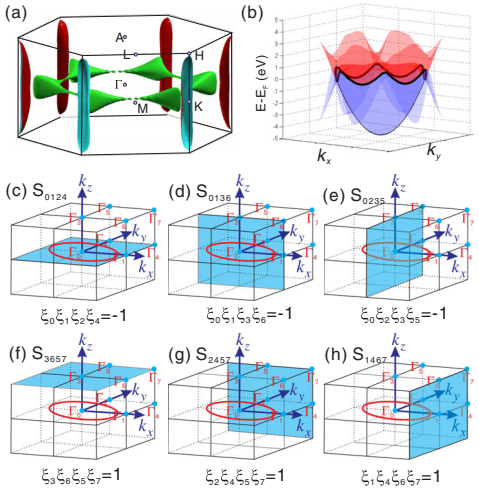

FIG. 2. Fermi surface, DNL, and six invariant S_{abcd} surfaces in the 3D BZ of hcp Be. (a) The Fermi surface in bulk hcp Be exhibits two-band features. (b) Illustration of the DNL, visualized by the two-band crossings. (c)–(h) Shaded regions represent three topologically nontrivial invariant planes (c)–(e) and three topologically trivial invariant planes (f)–(h). In (c)–(h), the red circle sketches the DNL.

coupling ($\lambda = 1.18$) [30] and giant Friedel oscillations [31] have been found at its (0001) surface. This fact along with the high density of states at the Fermi level was suggested to be a candidate to show surface superconductivity [29].

We start by representing the electronic structure of the bulk hcp Be phase [Fig. 1(a)] at the ground state within the framework of density functional theory (DFT) [38]. The derived electronic band structure of the hcp Be is shown in Fig. 1(c). It is quite similar to previous calculations [45]. We also derive the Fermi surface of its bulk phase in Fig. 2(a), in good accordance with the experimental measurement [46]. Its Fermi surface clearly consists of two parts: a coronetlike shape of six-cornered hole pockets on the $k_z = 0$ plane and a cigarlike shape of six equivalent electronic surfaces along the H-K symmetry direction. Nevertheless, a crucial feature was ignored in those previous studies. That is the appearance of two clear band crossings featured by a nearly linear dispersion around the Fermi level. One (crossing A) exactly locates at the Fermi level in the M-Γ direction and the other one (crossing B) lies about 0.8 eV above the Fermi level along the Γ-K direction. Actually, these two crossings are induced by the band inversion. At the center of the Brillouin zone (BZ) [see Fig. 1(b)] Γ, it can be seen that the band $s \to p_z$ inversion occurs between the no. 2 and no. 3 bands due to the crystal field effect [Fig. 1(c)]. Remarkably, the band crossings indeed not only appear at these two isolated A and B crossings, but also form a circlelike closed line around the Γ point on the $k_z = 0$ plane in the BZ. This is the exact sign of the DNL appearance. As elucidated in Fig. 2(b), the band crossings between no. 2 and no. 3 do not happen at the same energy, but show a periodic wavelike closed curve on the k vectors around the centered Γ point. In addition, this DNL's stability is highly robust, protected by the inversion and time-reversal symmetries without the spin-orbit coupling (SOC) effect. Because of the light mass of Be, its SOC effect is rather weak; therefore, it does not affect the electronic band structure [38].

We have calculated the Z_2 indices at the eight time-reversal invariant momentums (TRIMs) of Be, indicating that the product is $+1$ at Γ and -1 for all the other TRIMs (for details, refer to Ref. [38]). It evidences the occurrence of a band inversion at Γ and the DNL appearance around Γ. Then, we can obtain the Z_2 topological invariant $\omega(C_{abcd})$ of the six invariant S_{abcd} surfaces [21] (Fig. 2) following the recently proposed method [20,21] to identify the topology of the DNL states. Because the DNL pierces three nontrivial invariant surfaces [see Figs. 2(c)–2(e)], $\omega(C)$ is -1. However, $\omega(C)$ should be 1, as the other three trivial invariant surfaces [see Figs. 2(f)–2(h)] do not touch the DNL. Since the relation [21] is very similar to the topological invariants (v_0; v_1 v_2 v_3) of inversion-symmetric topological insulator [47], the Z_2 invariant in Be can be written as (1; 0 0 0).

To further elucidate the topological feature in beryllium, we have also constructed a 2×2 Hamiltonian within the framework of the low-energy $\boldsymbol{k}.\boldsymbol{p}$ model in describing two bands crossing, briefly. Using the $|s\rangle$ and $|p\rangle$ states as the bases, respecting time-reversal, and D_{6h} symmetries, the model Hamiltonian around Γ can be written as

$$H_\Gamma(\mathbf{k}) = \epsilon(\mathbf{k}) + \begin{pmatrix} M(\mathbf{k}) & B(\mathbf{k}) \\ B^\dagger(\mathbf{k}) & -M(\mathbf{k}) \end{pmatrix}, \quad (1)$$

where

$$\epsilon(\mathbf{k}) = \epsilon_0 + a_\parallel(k_x^2 + k_y^2) + a_\perp k_z^2, \quad (2)$$

$$M(\mathbf{k}) = m_0 + m_\parallel(k_x^2 + k_y^2) + m_\perp k_z^2, \quad (3)$$

$$B(\mathbf{k}) = B_0 k_z, \quad (4)$$

and the eigenvalues of the model Hamiltonian are $E(\mathbf{k}) = \epsilon(\mathbf{k}) \pm \sqrt{M^2(\mathbf{k}) + B^2(\mathbf{k})}$. In this case, the gapless solutions of Eq. (1), at which the Dirac node line would appear, can be yielded only when both $M(\mathbf{k})$ and $B(\mathbf{k})$ equal zero. Within this condition, on the $k_z = 0$ plane the node line locates at $|\mathbf{k}| = \pm\sqrt{-(m_0/m_\parallel)}$, which requires that $m_0 m_\parallel$ is always smaller than zero. This is also the condition of the band inversion occurrence. In other words, when band inversion happens, in the lack of SOC, there always exists a node line in the momentum space, which are the solutions of $M(\mathbf{k}) = B(\mathbf{k}) = 0$. Note that the band inversion only occurs at Γ among all TRIMs for Be according to the abovementioned topology analysis; a DNL would occur around the Γ point in agreement with the calculated electronic structure.

Using this Hamiltonian to describe the (0001) surface bands, the topologically nontrivial surface states could be expected. Since the (0001) surface is perpendicular to the c axis, we can use $-i\partial_z$ instead of k_z according to the theory of the linear order, and then the (0001) surface Hamiltonian can be expressed as follows:

$$H_\Gamma^{\text{surf}}(\mathbf{k}) = \epsilon_0 + a_\parallel k^2 + \begin{pmatrix} m_0 + m_\parallel k^2 & -iB_0\partial_z \\ iB_0\partial_z & -m_0 - m_\parallel k^2 \end{pmatrix}. \quad (5)$$

Becase of the Jackiw-Rebbi problem [48], there will be a topological boundary mode with the condition of $m_0 + m_\parallel k^2 < 0$. This suggests the presence of the topologically nontrivial surface states, which would nestle the projected Dirac node ring. To clarify this point, we calculate the surface electronic structures by varying the thickness of the slab as shown in Figs. 3(a)–3(f). As expected, the robust surface electronic bands [SF band 1 in Fig. 3(f)] appear when the slab's thickness is above 5 unit cells along the c axis. As shown in Fig. 3(f), from the crossing A to the B point the topological surface bands are twofold degenerated within the projected Dirac node ring. It can be seen that the topological surface bands along the $\overline{K}$-$\overline{\Gamma}$-$\overline{H}$ direction disperse parabolically from the lowest energy of −2.73 eV (experiment [26,46]: −2.80 and −2.75 eV, referred to as the Fermi level) at $\overline{\Gamma}$, and then cross the Fermi level at 51% (expt [46]: 49%) of the $\overline{\Gamma}$-$\overline{K}$ distance and 60% (expt [46]: 58%) of the $\overline{\Gamma}$-$\overline{M}$ distance, in good agreement with the experimental findings [see squares in Fig. 3(f)] obtained by ARPES [26,46]. In particular, it has been noted that the surface bands around the $\overline{\Gamma}$ and $\overline{M}$ points are highly different. The topologically protected SF band 1 around the $\overline{\Gamma}$ point is mainly composed with s- and p_z-like electronic states from the topmost atomic layer, reflecting well the crucial feature of the band inversion between s and p_z in its bulk phase [Fig. 1(c)]. This SF band 1 is indeed half filled when the surface is electrically neutral. The other two surface bands around $\overline{M}$ [SF band 2 and 3 in Fig. 3(f)] are the topologically trivial states, which are not correlated with the DNL state. SF band 2 is mainly composed with in-plane $p_{x,y}$-like electronic states from the topmost surface atomic layer, whereas the SF band 3 mainly consists of the $p_{x,y}$-like electronic states from the second outer atomic layer. Obviously, these SF bands, 2 and 3, are fully occupied when the surface is electronic neutral.

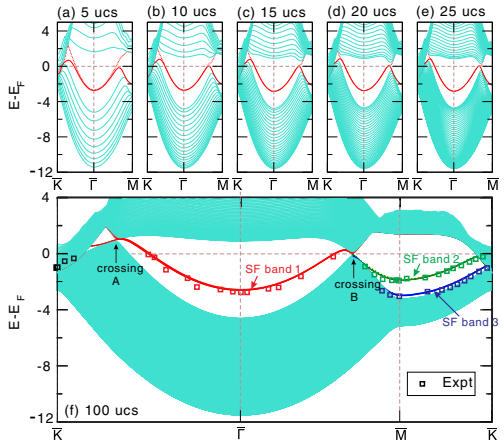

FIG. 3. The evolution of thickness-dependent surface electronic band structures of the Be (0001) surface. (a)–(e) The derived surface electronic structure is shown as a function of the slab thickness from 5 unit cells (ucs) to 25 ucs along the c axis with an increase of 5 ucs thickness in every image. (f) Surface electronic band structure with a slab thickness of 100 ucs, together with the experimentally measured data (squares [26]).

We have further derived its Fermi surface of the (0001) surface in Fig. 4(a). Because the DNL exists on the $k_z = 0$ plane in the BZ, the DNL projection onto the (0001) surface shows a closed circle [ring A in Fig. 4(a)] surrounding $\overline{\Gamma}$ within which the topologically protected surface bands [ring B in Fig. 5(a)] appear. Although ring B was already observed by ARPES [46] [Figs. 4(b) and 4(c)], it was not interpreted as the DNL-induced topologically nontrivial band. The understanding of the surface states [SF band 1 in Fig. 4(f) and ring B in Fig. 4(a)] has also been a long-standing question since the 1980s [26–34]. It was suspected to be correlated with unusually large outward relaxation of the topmost surface atoms, so-called p to s electron demotion as well as the core-level shifts [26–28,32–34]. However, those proposed mechanisms did not address the

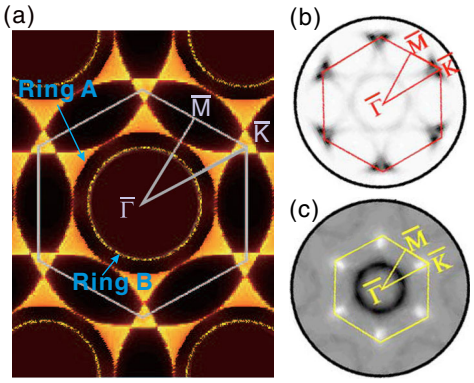

FIG. 4. Fermi surface of the Be (0001) surface. (a) DFT-derived Fermi surface highlighting a surface state of a fully closed circle around the centered $\bar{\Gamma}$ point in the Brillouin zone. The other parts are the projections of bulk bands. (b),(c) The experimentally measured Fermi surface (directly taken from Ref. [46]) cuts with $h\nu = 32.5$ and 86 eV, respectively, showing the difference between horizontal and vertical polarizations measured by the ARPES experiments.

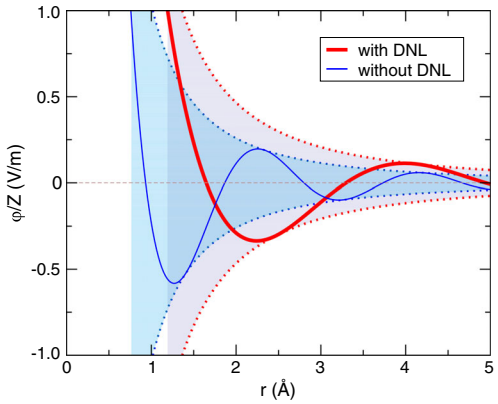

FIG. 5. The giant Friedel oscillation for the Be (0001) surface. The screened potential $\varphi(r)/Z$ is given as a function of the distance r. The red and blue solid curves denote the Friedel oscillation for the Be (0001) surface of the cases with and without DNL, respectively. The dashed red and blue curves denote the amplitude of $\varphi(r)/Z$.

underlying physical origin for the appearance and stability of the surface states [26]. Because of our calculations, the SF band 1 state is highly robust, no matter whether the surface slab modeling is relaxed or not [38]. Therefore, it is undoubtable that the SF band 1 is induced by the topological DNL feature in its bulk phase. Additionally, we would like to mention that, as early as in 1970, the Landau quantum oscillations of the magnetic susceptibility has been observed when the magnetic field was set to be parallel to the c-axis direction [49]. This seems to be another exciting sign to elaborate the DNL property in Be because the magnetic field certainly breaks the time-reversal symmetry and then gaps out the crossings to modify the Fermi surface.

Importantly, we have further found that the giant Friedel oscillation experimentally observed on the Be (0001) surface [31] can be interpreted by the DNL-induced topologically nontrivial surface states. We adopted a similar modeling recently used to interpret Friedel oscillations of topological materials [50–52]. For the Be (0001) surface, we use the screened potential of a charge impurity (Ze) of the two-dimensional electron gas (2DEG) system [53] that reads

$$\varphi(r) = -\frac{Zeq_s}{\kappa}\frac{1}{(2k_F + q_s)^2}\frac{\sin(2k_F r)}{r^2}, \qquad (6)$$

where $q_s = (gm^* e^2/\kappa\hbar^2)$, κ is the dielectric constant, r is the distance, k_F is the Fermi wave vector, and g is the degeneracy factor. This 2DEG system exhibits the so-called parabolic bands, which are highly similar to the topological nontrivial surface parabolic bands on the Be (0001) surface, as shown in Eq. (5). In the 2DEG system, $k_F = (2\pi\rho)^{1/2}$ (ρ is the electron density). However, in comparison with the 2DEG system, the k_F and q_s values must be highly different for the Be (0001) surface due to the existence of the DNL states. Using the 2DEG model to describe the Be (0001) surface by ignoring the topologically nontrivial surface feature (without DNL), k_F can be derived as 1.683 Å^{-1} because $\rho = (g/A)$, in which $g = 2$, denoting the two effective electrons (spin degeneracy) in the area (A) of the surface unit cell. However, with the inclusion of the topological surface bands (with DNL), as shown in Figs. 3(f) and 4(a), k_F is calculated to be 0.962 Å^{-1} (experiment [31]: 0.96 Å^{-1}) along the $\bar{\Gamma}$-$\bar{M}$ direction and $k_F = 0.944$ Å^{-1} (expt [31]: 0.93 Å^{-1}) along the $\bar{\Gamma}$-$\bar{K}$ direction. On average, the calculated k_F is about 0.953 Å^{-1} (expt [31]: 0.945 ± 0.02 Å^{-1}). As compared without DNL, k_F of the Be (0001) surface is much smaller in the real case with DNL. Additionally, the constant q_s is 4.80 Å^{-1} for the case without DNL, whereas in the case with DNL q_s is 2.40 Å^{-1}. Because the amplitude of the charge impurity screened potential is proportional to $q_s/(2k_F + q_s)^2$ in Eq. (6), the reduced k_F and q_s, that are induced by the half filled topologically nontrivial surface bands, definitely elevate the amplitude of the Friedel oscillation to be nearly twice that of without DNL, as illustrated in Fig. 5. In addition, another long-standing debate on the NFE deviation of the electronic structure of the Be (0001) surface has been clarified to also originate from the DNL [38].

Finally, we have also found a similar topological DNL feature in Mg, Ca, and Sr [38]. Mg is isostructural and isovalent to Be and their electronic band structures look highly similar to each other. In Mg (which is similar to Be) there also exists a DNL around the Fermi level, and the topologically protected nontrivial surface states are also obtained on the (0001) surface by surface calculations, which are also in good agreement with experiments [54].

Metals of Ca and Sr, which are isovalent to Be and Mg, crystallize in the fcc structure with the truncated octahedron BZ. These two metals also exhibit the DNL-like topological feature. On each hexagonal face of the BZ, the valence and conduction bands cross each other to form a closed loop that surrounds the center of the hexagonal face. Topological surface states can also be observed clearly on their symmetrically equivalent {111} surfaces. However, different from Be, their topological surface bands locate outside the projected DNLs because the band inversion occurs outside the DNLs.

In summary, we have discovered the 3D topological DNL states in the alkali earth metals (Be, Mg, Ca, and Sr), which has been confirmed in experiments through comparing the first-principles calculations and the photoemission spectroscopy, and clarified the long-standing debate on the anomalous electronic properties of the Be (0001) surface to be indeed correlated with the DNL states.

We thank H.-R. Chang, Y. G. Yao, and R. H. Hao for useful comments and discussions on the manuscript. This study was supported by the "Hundred Talents Project" of the Chinese Academy of Sciences, by the Key Research Program of Chinese Academy of Sciences (Grant No. KGZD-EW-T06), the National Natural Science Foundation of China (Grants No. 51474202, No. 51174188 and No. 91226204) and the high-performance computational cluster in the Shenyang National University Science and Technology Park.

Note added in proof.—Recently we became aware that Ca and Sr have been also reported to host the DNL states in Ref. [55].

*Corresponding author.
xingqiu.chen@imr.ac.cn

[1] M. Z. Hasan, S.-Y. Xu, and G. Bian, Phys. Scr. **T164**, 014001 (2015).
[2] S. M. Young, S. Zaheer, J. C. Y. Teo, C. L. Kane, E. J. Mele, and A. M. Rappe, Phys. Rev. Lett. **108**, 140405 (2012).
[3] X. Wan, A. M. Turner, A. Vishwanath, and S. Y. Savrasov, Phys. Rev. B **83**, 205101 (2011).
[4] S. Ryu and Y. Hatsugai, Phys. Rev. Lett. **89**, 077002 (2002).
[5] T. T. Heikkilä and G. E. Volovik, JETP Lett. **93**, 59 (2011).
[6] A. A. Burkov, M. D. Hook, and L. Balents, Phys. Rev. B **84**, 235126 (2011).
[7] Z. J. Wang, Y. Sun, X.-Q. Chen, C. Franchini, G. Xu, H. M. Weng, X. Dai, and Z. Fang, Phys. Rev. B **85**, 195320 (2012).
[8] Z. K. Liu, B. Zhou, Y. Zhang, Z. J. Wang, H. M. Weng, D. Prabhakaran, S. K. Mo, Z. X. Shen, Z. Fang, X. Dai, and Z. Hussain, Science **343**, 864 (2014).
[9] X. Y. Cheng, R. H. Li, Y. Sun, X.-Q. Chen, D. Z. Li, and Y. Y. Li, Phys. Rev. B **89**, 245201 (2014).
[10] S. Y. Xu, C. Liu, S. K. Kushwaha, R. Sankar, J. W. Krizan, I. Belopolski, M. Neupane, G. Bian, N. Alidoust, T. R. Chang, H. T. Jeng, C. Y. Huang, W. F. Tsai, H. Lin, P. P. Shibayev, F. C. Chou, R. J. Cava, and M. Z. Hasan, Science **347**, 294 (2015).
[11] Z. J. Wang, H. M. Weng, Q. S. Wu, X. Dai, and Z. Fang, Phys. Rev. B **88**, 125427 (2013).
[12] M. Neupane, S. Y. Xu, R. Sankar, N. Alidoust, G. Bian, C. Liu, I. Belopolski, T. R. Chang, H. T. Jeng, H. Lin, A. Bansil, F. Chou, and M. Z. Hasan, Nat. Commun. **5**, 3786 (2014).
[13] Z. K. Liu, J. Jiang, B. Zhou, Z. J. Wang, Y. Zhang, H. M. Weng, D. Prabhakaran, S. K. Mo, H. Peng, P. Dudin, T. Kim, M. Hoesch, Z. Fang, X. Dai, Z. X. Shen, D. L. Feng, Z. Hussain, and Y. L. Chen, Nat. Mater. **13**, 677 (2014).
[14] H. M. Weng, C. Fang, Z. Fang, B. A. Bernevig, and X. Dai, Phys. Rev. X **5**, 011029 (2015).
[15] S. M. Huang, S. Y. Xu, I. Belopolski, C. C. Lee, G. Q. Chang, B. K. Wang, N. Alidoust, G. Bian, M. Neupane, C. L. Zhang, S. Jia, A. Bansil, H. Lin, and M. Z. Hasan, Nat. Commun. **6**, 7373 (2015).
[16] B. Q. Lv, H. M. Weng, B. B. Fu, X. P. Wang, H. Miao, J. Ma, P. Richard, X. C. Huang, L. X. Zhao, G. F. Chen, Z. Fang, X. Dai, T. Qian, and H. Ding, Phys. Rev. X **5**, 031013 (2015).
[17] S. Y. Xu *et al.*, Science **349**, 613 (2015).
[18] A. A. Soluyanov, D. Gresch, Z. J. Wang, Q. S. Wu, M. Troyer, X. Dai, and B. A. Bernevig, Nature (London) **527**, 495 (2015).
[19] H. M. Weng, Y. Y. Liang, Q. N. Xu, R. Yu, Z. Fang, X. Dai, and Y. Kawazoe, Phys. Rev. B **92**, 045108 (2015).
[20] R. Yu, H. M. Weng, Z. Fang, X. Dai, and X. Hu, Phys. Rev. Lett. **115**, 036807 (2015).
[21] Y. Kim, B. J. Wieder, C. L. Kane, and A. M. Rappe, Phys. Rev. Lett. **115**, 036806 (2015).
[22] L. S. Xie, L. M. Schoop, E. M. Seibel, Q. D. Gibson, X. X. Xie, and R. J. Cava, APL Mater. **3**, 083602 (2015).
[23] M. G. Zeng, C. Fang, G. Q. Chang, Y.-A. Chen, T. Hsieh, A. Bansil, H. Lin, and L. Fu, arXiv:1504.3492.
[24] L. Lu, L. Fu, J. D. Joannopoulos, and M. Soljaćić, Nat. Photonics **7**, 294 (2013).
[25] K. Mullen, B. Uchoa, and D. T. Glatzhofer, Phys. Rev. Lett. **115**, 026403 (2015).
[26] E. W. Plummer and J. B. Hannon, Prog. Surf. Sci. **46**, 149 (1994).
[27] U. O. Karlsson, S. A. Flodstrom, R. Engelhardt, W. Gadeke, and E. E. Koch, Solid State Commun. **49**, 711 (1984).
[28] R. A. Bartynski, E. Jensen, T. Gustafsson, and E. W. Plummer, Phys. Rev. B **32**, 1921 (1985).
[29] M. Hengsberger, D. Purdie, P. Segovia, M. Garnier, and Y. Baer, Phys. Rev. Lett. **83**, 592 (1999).
[30] T. Y. Chien, X. B. He, S.-K. Mo, M. Hashimoto, Z. Hussain, Z.-X. Shen, and E. W. Plummer, Phys. Rev. B **92**, 075133 (2015).
[31] P. T. Sprunger, L. Petersen, E. W. Pulmmer, E. Laegsgaard, and F. Besenbacher, Science **275**, 1764 (1997).
[32] H. L. Davis, J. B. Hannon, K. B. Ray, and E. W. Plummer, Phys. Rev. Lett. **68**, 2632 (1992).
[33] L. I. Johansson, H. I. P. Johansson, J. N. Andersen, E. Lundgren, and R. Nyholm, Phys. Rev. Lett. **71**, 2453 (1993).

[34] P. J. Feibelman, Phys. Rev. B **46**, 2532 (1992).
[35] K. J. H. Mackay and N. A. Hill, J. Nucl. Mater. **8**, 263 (1963).
[36] N. Marzari, D. Vanderbilt, A. De Vita, and M. C. Payne, Phys. Rev. Lett. **82**, 3296 (1999).
[37] J.-H. Cho, Ismail, Z. Y. Zhang, and E. W. Plummer, Phys. Rev. B **59**, 1677 (1999).
[38] See Supplemental Material at http://link.aps.org/supplemental/10.1103/PhysRevLett.117.096401 for (1) computational details (which includes Refs. [39–44]), (2) parities of occupied bands in hcp Be, (3) impact of surface structural relaxation on topological surface electronic bands, (4) DNL mechanism of the severe deviation from the NFE model, (5) DNLs in hcp Mg and fcc Ca (Sr), and (6) SOC effect on the DNLs in Be, Mg, Ca, and Sr.
[39] P. Hohenberg and W. Kohn, Phys. Rev. **136**, B864 (1964).
[40] W. Kohn and L. J. Sham, Phys. Rev. **140**, A1133 (1965).
[41] G. Kresse and J. Furthmüller, Phys. Rev. B **54**, 11169 (1996).
[42] P. E. Blöchl, Phys. Rev. B **50**, 17953 (1994).
[43] D. C. Langreth and M. J. Mehl, Phys. Rev. B **28**, 1809 (1983).
[44] J. P. Perdew, K. Burke, and M. Ernzerhof, Phys. Rev. Lett. **77**, 3865 (1996).
[45] M. Y. Chou, P. K. Lam, and M. L. Cohen, Phys. Rev. B **28**, 4179 (1983).
[46] I. Vobornik, J. Fujii, M. Mulazzi, G. Panaccione, M. Hochstrasser, and G. Rossi, Phys. Rev. B **72**, 165424 (2005).
[47] L. Fu, C. L. Kane, and E. J. Mele, Phys. Rev. Lett. **98**, 106803 (2007).
[48] R. Jackiw and C. Rebbi, Phys. Rev. D **13**, 3398 (1976).
[49] L. R. Testardi and J. H. Condon, Phys. Rev. B **1**, 3928 (1970).
[50] P. Hosur, Phys. Rev. B **86**, 195102 (2012).
[51] H.-R. Chang, J. H. Zhou, H. Zhang, and Y. G. Yao, Phys. Rev. B **89**, 201411 (2014).
[52] M. Lv and S.-C. Zhang, Int. J. Mod. Phys. B **27**, 1350177 (2013).
[53] F. Stern, Phys. Rev. Lett. **18**, 546 (1967).
[54] U. O. Karlsson, G. V. Hansson, P. E. S. Persson, and S. A. Flodström, Phys. Rev. B **26**, 1852 (1982).
[55] M. Hirayama, R. Okugawa, T. Miyake, and S. Murakami, arXiv:1602.06501.